MM Science Journal | www.mmscience.eu
ISSN 1803-1269 (Print) | ISSN 1805-0476 (On-line)
Special Issue | CUTTING TOOLS 2024
1st International Conference on Cutting Tools
November 20-24, 2024, Trnava, Slovakia
DOI: 10.17973/MMSJ.2025_03_2025014

CUTTINGTOOLS2024-00004

EFFECT OF WAAM PARAMETERS ON THE ALUMINUM ALLOY SINGLE LAYER BEAD GEOMETRY

M. Pavlik[1]*, B. Ludrovcova[1], Martin Sahul[1], Miroslav Sahul[2], J. Kotianova[1]

[1]Slovak University of Technology in Bratislava, Faculty of Materials Science and Technology in Trnava, Slovak Republic

[2]Czech Technical University in Prague, Faculty of Mechanical Engineering, Prague, Czech Republic

*Corresponding author; e-mail: marian.pavlik@stuba.sk

Abstract
This study investigates the impact of process parameters on the geometry of single-layer overlay welds of AA5087 aluminum alloy, fabricated using Wire and Arc Additive Manufacturing (WAAM-MIG), a technique valued for its productivity and material efficiency. This method layers material as weld beads to build 3D structures. Key characteristics analyzed include bead width, bead height, penetration depth, porosity, and costs related to shielding gas flow rates. Using the Taguchi method with an L27 orthogonal array, the study optimized experimental designs while reducing trial numbers. Grey relational analysis enabled the simultaneous evaluation of multiple parameters. Optimization was conducted for individual responses and through multi-objective analysis to determine the significance of parameters for each characteristic. The findings enhance understanding of the WAAM-MIG process and its application in manufacturing components with precise geometric characteristics, supporting advancements in additive manufacturing.

Keywords:
Taguchi method, individual optimization, multi-objective optimization, grey relation analysis

1 INTRODUCTION

Wire and Arc Additive Manufacturing (WAAM) utilizes a welding arc to melt and deposit metal wire in layers, enabling high deposition rates and cost-effective additive manufacturing, particularly for aluminum alloys in aerospace, automotive, marine, and energy sectors [Singh et al., 2021]. The process involves robotic systems stacking molten metal beads to form each layer, with the filler wire melted by an electric arc and deposited as metal droplets along a predefined path [Sarıkaya et al., 2024]. Since Al-Mg alloys cannot be heat-treated, their mechanical properties depend entirely on process parameters, making parameter selection crucial to achieving the desired bead shape and minimizing defects [Prasad et al., 2024; Sarikaya et al., 2024]. The optimization of these parameters has been the focus of numerous studies, utilizing techniques such as Response Surface Methodology (RSM), Design of Experiment (DOE), and Artificial Neural Networks (ANNs) [He et al., 2024; Lee et al., 2020; Mohd Mansor et al., 2024; Singla et al., 2024]. Research by Manikandan et al. [2024] optimized the GMAW-CMT WAAM method of Al5356, achieving defect-free beads with optimal settings of welding current 135 A, welding voltage 16 V, and an overlay welding speed of 40 cm/min. Similarly, Kazmi et al. [2024] used Central Composite Design to optimize bead deposition of ER-4043 on an Al 6063 substrate, finding that higher overlay welding speeds improved bead height but increased surface roughness. Shams et al. [2024] and Du et al. [2023] investigated the effects of voltage, scanning speed, and energy density on porosity and bead geometry in WAAM, while Srinivas et al. [2022] applied a Taguchi L9 orthogonal array to analyze wire feed rate, gas flow rate, and overlay welding speed in WAAM of ER5356 alloy. This paper examines the influence of WAAM process input parameters – overlay welding speed, wire feed speed, and shielding gas flow rate - on bead width, bead height, penetration depth, porosity, and the associated costs of shielding gas flow rate.

2 MATERIALS AND METHODS

2.1 Chemical composition of materials, workplace and device

The selected filler material was a wire with a diameter of 1.2 mm. The chemical composition of the wire is provided in Tab. 1. Trace amounts of manganese in aluminum alloys of the 5xxx series form dense dispersoids with improved homogeneity, contributing to dispersion strengthening. Specifically, 5087 alloy is also alloyed with zirconium, which enhances resistance to hot cracking. Zirconium also has the function of grain size control (microstructure refinement), thereby improving mechanical properties such as strength, toughness, and resistance to fatigue, stress, and corrosion. According to Wang et al. and Pourkia et al., zirconium may also reduce porosity [Pourkia, N. 2010] [Wang, J. 2009].

Tab. 1: Chemical composition of AA5087 filler material (wt.%).

Si	Fe	Cu	Mn	Mg	Cr	Zn	Zr	Ti	Be	Al
≤0.4	≤0.40	≤0.1	0.4-1.1	4.5-5.2	0.05-0.25	≤0.25	0.10-0.2	≤0.15	≤0.0003	Bal.

The substrate had dimensions of 100 × 200 × 4 mm. The chemical composition of the substrate is given in Tab. 2. The surface of the substrate was cleaned with a steel brush and acetone before the first layer was applied to achieve the desired contact area with the filler material.

Tab. 2: Chemical composition of AA5083 base material (wt.%).

Cu	Fe	Zn	Ti	Mn	Cr	Si	Mg	Al
≤0.1	≤0.4	≤0.25	≤0.15	0.5-1	0.05-0.25	≤0.4	4-4.9	Bal.

The experiments were conducted at the Arc and Plasma Technologies Laboratory, as illustrated in Fig. 1. The setup features a rigid substrate clamping system that prevents excessive deformation, thereby enhancing the quality of the deposited layer. The welding power source used was a Fronius TPS600i, capable of delivering a maximum welding current of 600 A. The welding torch is connected to the welding system for parameter control and is mounted on a manipulator gantry. The reach of the gantry defines the maximum dimensions of the manufactured component.

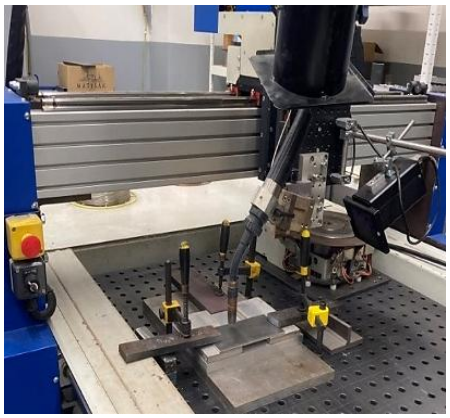

Fig. 1: Workplace for Wire and Arc Additive Manufacturing of AA5087.

2.2 Principle of statistical analysis, statistical responses and sample preparation

The path programming was performed using a relative coordinate system, which references the last waypoint of the preceding motion path. The trajectory that the heat source or deposition system must follow is determined by the final profile of the component. In the case of a controlled manipulator gantry, the path is tracked along three axes: x, y, and z. The analysis of the experimental data is carried out using the MiniTab 19 software specially used for design of experiment applications. The experimental design was carried out on 80 mm long beads. Each of the beads was cut into 3 parts, based on the scheme in Fig. 2. The green arrows show the direction of sample analysis.

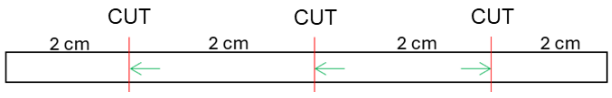

Fig. 2: Schematic representation of sample preparation for design of experiment.

Schematic illustration of WAAM build and deposition directions is shown in Fig. 3.

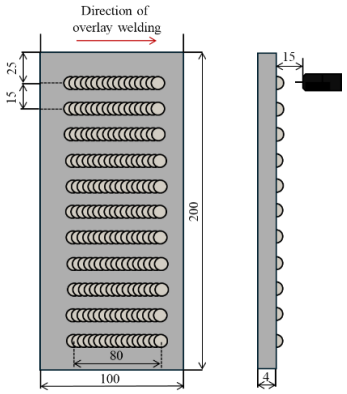

Fig. 3: Schematic illustration of WAAM build and deposition directions.

The principle of data acquisition for statistical analysis is illustrated in Fig. 4. The red line represents the penetration depth, which measures the extent to which the deposited material was fused with the base material (AA5083). The green line indicates the height of the bead, which corresponds to the vertical build-up of the filler material (AA5087) above the substrate. The blue line characterizes the width of the bead, which defines the lateral spread of the deposited material. Additionally, the figure highlights the presence of pores within the deposited layer, with specific indications of features considered as pores and those excluded from pore analysis. These parameters penetration depth, bead height, and bead width are critical for evaluating the geometric and mechanical quality of the overlay weld. The porosity of the WAAM-fabricated AA5087 alloy was evaluated using image thresholding in ImageJ. The IsoData method was applied, setting the threshold range from 0 to 70 to distinguish pores from the solid material. The selected threshold ensured accurate segmentation of porosity for further quantitative analysis. Based on the previous macroscopic analysis, the layer height can be estimated at approximately 2 mm, while the layer width is around 7.5 mm, depending on the applied process parameters.

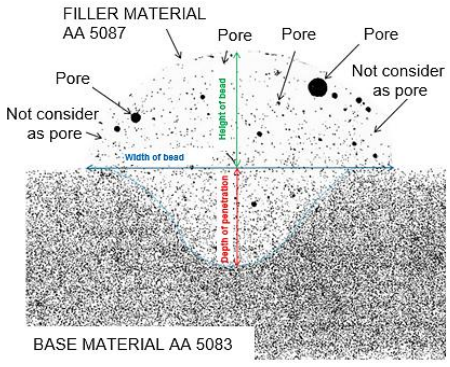

Fig. 4: Principle of data collection for statistical analysis by Taguchi L27 method.

A cost model calculation associated with shielding gas flow depends on the length of the deposited bead, which was 80 mm. The shielding gas cylinder has a volume of 50 litres, and its price was €42. For a deposition speed of 4 mm/s, the cylinder's usage time for this speed is 20 seconds, with a gas flow rate of 12 l/min. The calculation is based on the following formula:

$$p_1 \times V_1 = p_2 \times V_2 \quad (1)$$

where p_1 is initial gas pressure in the cylinder, V_1 cylinder volume, p_2 is atmospheric pressure when the gas is

released and V_2 is gas volume after expansion to atmospheric pressure.

Using this formula, it was determined that the cylinder contains 10 000 litres of shielding gas. To produce a single deposited bead, 4 litres of shielding gas are consumed. The cost of 1 liter of gas is €0.0042. Therefore, a single bead produced with the given parameters consumes shielding gas costing €0.0168.

3 RESULTS

The investigated characteristics were width of bead, height of bead, depth of penetration, porosity, and cost associated with gas flow rate. The bead parameters highlighted in yellow were selected for statistical analysis by Taguchi's L27 method based on grey relational analysis. Fig. 5 shows the 33 beads that were produced for statistical analysis. The beads were made with different overlay welding speed (OWS), wire feed speed (WFS) and gas flow rate (GFR). A total of 33 single-layers WAAM deposits were fabricated, varying key process parameters. For the Taguchi L27 experimental design, nine representative samples were selected based on their geometric consistency, bead integrity, and uniformity of the start and end regions. Additionally, the selected parameter combinations were spaced apart sufficiently to ensure distinct variations in process behavior, facilitating a clearer evaluation of their influence on bead formation and overall deposition quality.

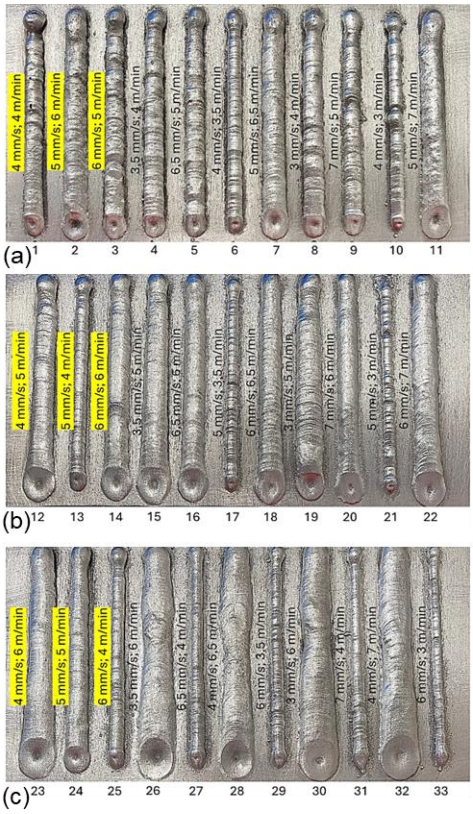

Fig. 5: 33 beads prepared for Taguchi L27 statistical analysis.

The input data analyzed for individual parameters within the separate optimization in Minitab are presented in Tab. 3. The analyzed values for OWS were 4, 5, and 6 mm/s. For WFS also 4, 5 and 6 m/min. For GFR, the analyzed values were 8, 12 and 16 l/min. The weight values (w) were set uniformly at 0.2 to better assess the influence of each response, with the total weight of the entire decision-making process equal to 1. The maximum value of bead width was 11.333 mm with OWS value 4 mm/s, WFS value 6 m/min, and GFR value 16 l/min. On the other hand, the smallest bead width was 4.42 mm with OWS value 6 mm/s, WFS value 4 m/min, and GFR value 16 l/min. The highest porosity of 19.28% was recorded at the OWS value 4 mm/s, WFS value 4 m/min, and GFR value 8 l/min. The lowest level of porosity was found at OWS of 5 mm/s, WFS of 5 m/min, and GFR of 16 l/min, namely 0.19%. During the measurements, constant welding parameters were maintained. The current used in the experiment was set to 65 A, while the voltage remained stable at 16,1 V. Additionally, the distance between the welding torch and the deposited layer was kept constant at 15 mm. These conditions ensured the reproducibility of the results and minimized the influence of external factors on the measured variables.

Tab. 3: Measured data for the evaluation of Taguchi's L27 method.

Overlay welding speed (mm/s)	Wire feed speed (m/min)	Gas flow rate (l/min)	Width of bead (mm)	Height of bead (mm)	Depth of penetration (mm)	Porosity (%)	Costs (€)
A	B	C	w=0.2	w=0.2	w=0.2	w=0.2	w=0.2
4	4	8	5.857	3.39	1.419	4.45	0.01121
4	4	8	6.261	3.311	1.123	15.63	0.01121
4	4	8	5.825	4.188	0.768	19.28	0.01121
4	5	12	8.246	3.116	2.246	1.29	0.0168
4	5	12	7.276	2.653	2.58	0.96	0.0168
4	5	12	9.682	2.856	4.119	0.68	0.0168
4	6	16	11.333	3.362	4.275	0.61	0.02239
4	6	16	10.85	3.095	4.38	0.86	0.02239
4	6	16	8.12	2.727	2.945	1.02	0.02239
5	4	12	4.827	3.391	0.654	5.13	0.01344
5	4	12	5.436	3.363	0.783	2.51	0.01344
5	4	12	5.652	2.928	0.855	4.87	0.01344
5	5	16	7.101	3.203	1.551	2.69	0.01793
5	5	16	8.074	3.017	2.405	1.07	0.01793
5	5	16	8.15	2.727	2.989	0.19	0.01793
5	6	8	6.54	2.465	2.134	3.78	0.00899
5	6	8	7.277	2.653	2.614	0.97	0.00899
5	6	8	7.536	2.681	2.435	2.39	0.00899
6	4	16	4.551	2.972	0.551	2.01	0.01495
6	4	16	4.42	2.87	0.725	1.83	0.01495
6	4	16	5.247	2.639	1.294	0.65	0.01495
6	5	8	9.435	3.275	4.464	1.94	0.00748
6	5	8	9.059	3.348	4.29	3.26	0.00748
6	5	8	9.58	2.987	4.768	2.95	0.00748
6	6	12	9.116	2.783	2.435	1.12	0.01121
6	6	12	9.625	2.683	3.104	0.54	0.01121
6	6	12	9.669	2.61	3.161	0.48	0.01121
		max	11.333	4.188	4.768	19.28	0.02239
		min	4.42	2.465	0.551	0.19	0.00748

3.1 Individual optimization

In the first step of optimization based on the Design of Experiment (DoE), the optimization was performed separately for each response to identify the most critical factors for individual performance parameters. Individual optimization allows for a clearer understanding of how specific factors contribute to changes in the response and how they may vary under different conditions. It also facilitates better parameter tuning and model refinement before applying more complex methods. For each response, two types of ANOVA statistical test will be analyzed under individual optimization. The first table, “Analysis of Variance for SN ratios”, focuses on signal-to-noise (SN) ratios, which are commonly used in robust design to evaluate the stability and quality of a process. SN ratios help identify factors that minimize variability and improve consistency under varying conditions. The second table, “Analysis of Variance for Means”, analyzes the mean values of the bead width. This approach evaluates the direct impact of factors on the average performance of the process. By combining these methods, it is possible to optimize the process for both stability and performance. Since it is not possible to determine whether a smaller or larger value is ideal in this case, the optimization will be performed using the “nominal is best” approach, where the nominal value was set to 7.5 mm. This value was derived

from the average of the measured bead width values of single-layer overlays. In Tab. 4, it is possible to see that none of the factors (A, B, C) have a statistically significant effect on bead width, as all P-values are greater than 0.05.

Tab. 4: ANOVA for SN ratios of bead width (7.5 mm).

Analysis of Variance for SN rations (width of bead = 7,5mm)

Source	DF	Seq SS	Adj SS	Adj MS	F-value	P-value
A	2	77,528	77,528	38,7642	1,16	0,464
B	2	1,199	1,199	0,5997	0,02	0,982
C	2	89,33	89,33	44,665	1,33	0,429
Residual Error	2	67,006	67,006	33,503		
Total	8	235,06				

Tab. 5 shows the significant effect of factor B (wire feed speed) with P-value = 7E-07, indicating a strong influence on the bead width. The highest F-value found for this case was 31.336, with a corresponding p-value and an overall contribution of 67.93%, attributed to the wire feed speed in m/min. Also, the overlay welding speed showed statistical significance (0.02) with a percentage contribution of 10.10. The percentage contribution to the gas flow rate was 0.28, making the contribution so small as to be statistically insignificant.

Tab. 5: ANOVA for Means of bead width.

Analysis of Variance for Means (width of bead)

Source	DF	SS	MS	F-value	P-value
A	2	10,187	5,0935	4,661	0,0218
B	2	68,487	34,244	31,336	7E-07
C	2	0,286	0,143	0,1309	0,8781
Error	20	21,856	1,0928		
Total	26	100,82			

The main effects plot for the S/N ratio (bead width) is shown in Fig. 6. If a parameter is located near the dashed line, it indicates that its influence on bead width is minimal. Parameters with steeper slopes have a more significant impact on bead width, specifically the welding speed and gas flow rate. Based on this, the optimal conditions were identified as A3B3C1, maximizing the system's robustness.

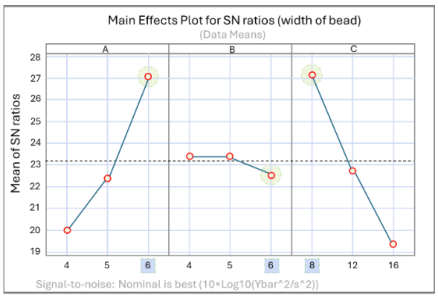

Fig. 6: Main effects plot for SN ratios of bead width.

The main effects plot in Fig. 7 evaluates the average effects of factors on the output variable, without considering variability or robustness to noise, from a classical DoE experimental design. The value against which the main effects plot was evaluated was set to 7.5 mm (green line). Fig. 8 shows contour plots of the regression analysis to check the quality of the model and its assumptions. Checks were made for the normal distribution condition, homoscedasticity, and the behavior of the residuals in time. The red line appears to go through the data, indicating a good fit to the normal, but there are clusters of plotting points at the same measured value [Kumar, P.B.K. 2021] [Sesharao, Y. 2021]. It means that multiple measurements are taking similar values. This occurs on a probability plot when there are many ties in the data. Moreover, the p-values exceeded 0.05 (A = 0.46, B = 0.98 and C = 0.43), indicating no statistical evidence against the assumption of normality. The shape of the histogram is not typical. This is probably due to the low number of data or their specific grouping (by rounding the values). To determine whether the input parameters influence the output results, a graphical analysis of residuals was used. Residuals, plotted on the y-axis, were compared against the fitted (predicted) values on the x-axis in the Versus Fit graph. The residuals are randomly scattered around zero (within ± 3σ), indicating constant variance and compliance with the assumption of homoscedasticity. Points located both higher and lower in the graph are horizontally oriented, while some points are distributed more freely along the residual line (zero value). The Versus Order graph was utilized to detect autocorrelation of residuals (y-axis) in relation to the observation order (x-axis). It can be observed that the residuals are randomly scattered around the zero line, showing no systematic trend. It can be concluded that all values fall within the control range, indicating no obvious pattern or unusual structure. Additionally, the residual analysis does not suggest any model inadequacy. Therefore, these values are expected to produce better results in future predictions.

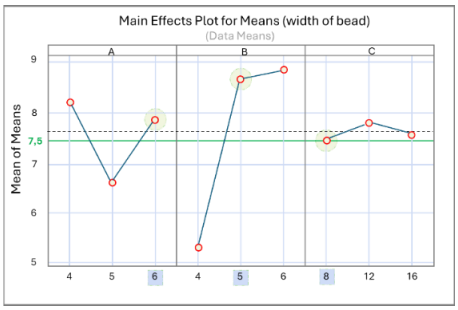

Fig. 7: Main effects plot for Means of bead width.

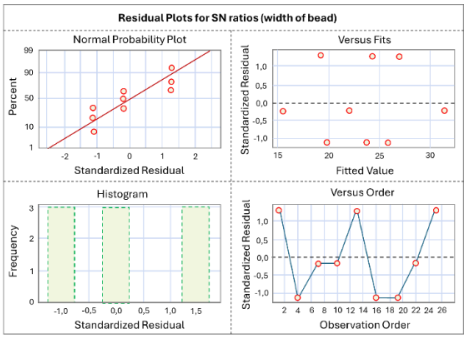

Fig. 8: Residual plots for SN ratios of bead width

The ANOVA for the SN ratios corresponding to a height bead of 3 mm is presented in Tab. 6. It can be observed that neither of the factors is statistically significant.

Tab. 6: ANOVA for SN ratios of bead height (3 mm).

Analysis of Variance for SN rations (heigh of bead = 3mm)

Source	DF	Seq SS	Adj SS	Adj MS	F-value	P-value
A	2	65,579	65,579	32,789	7,75	0,114
B	2	27,263	27,263	13,632	3,22	0,237
C	2	9,929	9,929	4,964	1,17	0,46
Residual Error	2	8,464	8,464	4,232		
Total	8	111,235				

Based on ANOVA for Means of bead height, a significant effect of factor B (wire feed speed) can be seen, with a p-value of 0.02642. This represents a contribution of 24.74%. Factor A and C are non-significant.

Tab. 7: ANOVA for Means of bead height.

Analysis of Variance for Means (heigh of bead)

Source	DF	SS	MS	F-value	P-value
A	2	0,4306	0,2153	2,12705	0,145361
B	2	0,887	0,4435	4,38155	0,026420
C	2	0,243	0,1215	1,20036	0,321871
Error	20	2,0244	0,10122		
Total	26	3,585			

The best circumstances based on the main effects plot for height of bead (SN ratios) were classified as A3B3C2 (Fig. 9). The smallest effect of undesirable variability is observed for factor A (overlay welding speed).

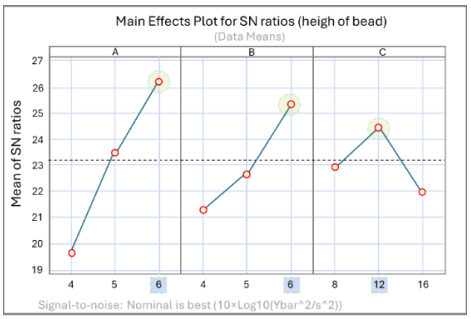

Fig. 9: Main effects plot for SN ratios of bead height.

The main effects plot for Means (Fig. 10) shows the factors for a specific mean value of 3 mm (green line). Parameters that produce mean values closer to this target are preferred for optimizing the process. The highlighted points on the plot indicate the levels where the response is closest to the target, providing guidance for selecting the most suitable process conditions. Each parameter's effect on the response is visualized by the slope of the line connecting the levels. For the first factor A, the response decreases significantly from the first level to the second level and then remains nearly constant between the second and third levels. This indicates that the first parameter does not have such a pronounced effect between its initial levels but becomes bigger influential at higher levels. In factor B, the response decreases sharply from the first level to the second level, followed by a steep decrease from the second level to the third level. This suggests that the second parameter has a strong influence on the response. In factor C, from first to second level followed by a decrease, the response remains relatively constant between the second and third levels. This indicates that the third parameter has a major influence at lower levels. A2B2C3 can be considered the most optimal.

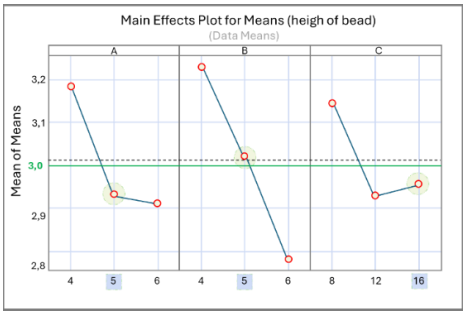

Fig. 10: Main effects plot for Means of bead height.

Fig. 11 shows residual plots for SN ratios for height of bead. The normal probability plot exhibits data points aligning closely with a straight line, indicating that the data follows a normal distribution. Additionally, the histogram of residuals reveals no significant deviations, suggesting the absence of outliers within the dataset. Versus fits plot presents that data points appear randomly dispersed without any discernible pattern. This suggests the absence of a linear relationship between the variables.

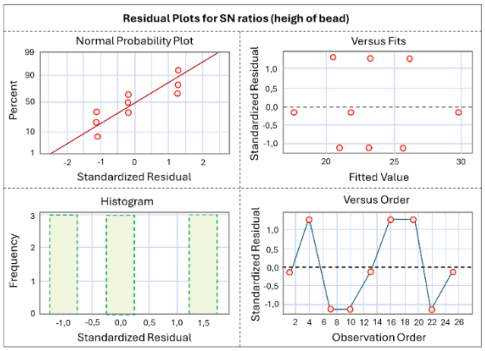

Fig. 11: Residual plots for SN ratios of bead height.

An analysis of variance (ANOVA) was conducted on the signal-to-noise (SN) ratios for penetration depth (Tab. 7). The evaluation was performed using the nominal is best criterion, with a target penetration depth of 2 mm. The statistical analysis indicated that none of the examined factors had a significant effect on the response variable, suggesting that variations in the penetration depth were not systematically influenced by the studied factors.

Tab. 7: ANOVA for SN ratios of penetration depth (2 mm).

Analysis of Variance for SN rations (penetration depth = 2mm)

Source	DF	Seq SS	Adj SS	Adj MS	F-value	P-value
A	2	48,44	48,44	24,22	0,57	0,638
B	2	42,34	42,34	21,17	0,5	0,669
C	2	106,22	106,22	53,11	1,24	0,446
Residual Error	2	85,41	85,41	42,7		
Total	8	282,4				

As a result, an analysis of means was conducted to further investigate potential differences among factor levels. This approach allows for the identification of deviations from the overall means and provides additional insights into the effects of individual factors, particularly in cases where ANOVA does not indicate statistically significant differences (Tab. 7). Tab. 8 presents the statistical analysis results, indicating a significant effect of factors A and B ($p < 0.05$). Factor B exhibited the highest contribution, accounting for 64.96% of the total variation, while factor A contributed 9.91%. In contrast, factor C was determined to be non-significant, with a minimal contribution of only 2.07%.

Tab. 8: ANOVA for Means of penetration depth.

Analysis of Variance for Means (penetration depth)

Source	DF	SS	MS	F-value	P-value
A	2	4,676	2,338	4,29693	0,0280268
B	2	30,66	15,33	28,1745	1,5215E-06
C	2	0,9788	0,4894	0,89945	0,42262382
Error	20	10,8822	0,54411		
Total	26	47,197			

Fig. 12 illustrates the main effects plot for SN ratios and Fig. 13 describes the main effects plot for means of penetration depth. For signal-to-noise (S/N) ratios, the optimal conditions were identified as A3B3C1. In contrast, for the mean response, the most favourable conditions, defined as those closest to the target value of 2 mm (represented by the green line), were determined to be A2B3C2. The factor exerting the greatest influence on the S/N ratios was the gas flow rate.

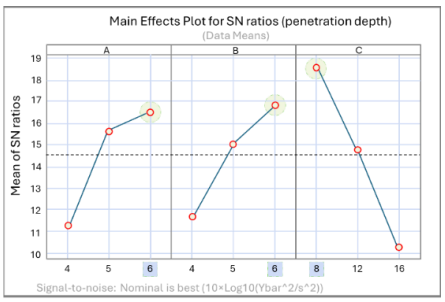

Fig. 12: Main effects plot for SN ratios of penetration depth.

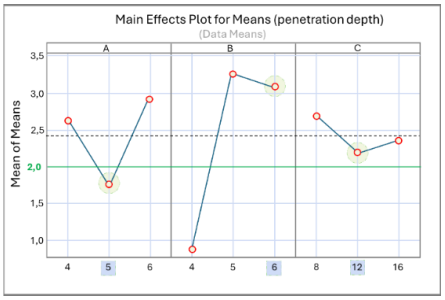

Fig. 13: Main effects plot for Means of penetration depth.

Residual plots for SN ratios for penetration depth is presented in Fig. 14. The normal probability plot demonstrates that the data points align closely with a straight line, suggesting that the data follows a normal distribution. However, the histogram of residuals reveals a slight deviation, with one value (1.5) differing from the overall pattern. This observation may indicate a minor anomaly in the residual distribution, though it does not necessarily suggest a significant departure from normality. The versus fits plot illustrates that the data points are randomly distributed, exhibiting no apparent systematic pattern, which suggests that the model residuals do not display heteroscedasticity or autocorrelation.

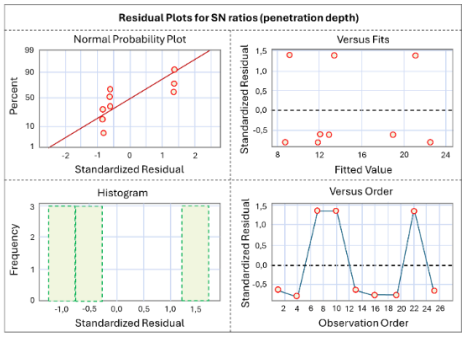

Fig. 14: Residual plots for SN ratios of penetration bead.

Weld porosity is a defect resulting from the entrapment of gas bubbles within the solidifying metal seam during the welding process. Consequently, porosity was assessed with the objective of minimizing it, where smaller values are preferred. Based on the ANOVA analysis for signal-to-noise (S/N) ratios, no significant effect of either factor was observed, as shown in Tab. 9. Factor A was determined to have the least influence on porosity, with a system robustness value of 0.408. For the ANOVA test for means, factors B and C were found to be significant, with contributions of 27.28% and 24.5%, respectively. These results suggest that both factors have a considerable impact on the observed variation in the data. Factor B, with its higher percentage, may play a more dominant role in influencing the outcome, while factor C also contributes significantly but to a lesser extent, as reported Tab. 10.

Tab. 9: ANOVA for SN ratios of porosity (smaller is better).

Analysis of Variance for SN rations (porosity = smaller is better)

Source	DF	Seq SS	Adj SS	Adj MS	F-value	P-value
A	2	40,08	40,08	20,04	1,45	0,408
B	2	227,36	227,36	113,68	8,24	0,108
C	2	225,2	225,2	112,6	8,16	0,109
Residual Error	2	27,58	27,58	13,79		
Total	8	520,23				

Tab. 10: ANOVA for Means of porosity.

Analysis of Variance for Means (pórovitosť)

Source	DF	SS	MS	F-value	P-value
A	2	52,83	26,415	2,78302	0,08583542
B	2	137,3	68,65	7,23279	0,00432957
C	2	123,3	61,65	6,49529	0,00670505
Error	20	189,83	9,4915		
Total	26	503,26			

To minimize porosity, the evaluation criterion was based on the “Smaller is better” signal-to-noise (S/N) ratio. The main effects plot (Fig. 15) shows an increasing trend in response values at higher levels of the examined factors. This suggests that increasing certain parameters leads to a rise in the measured quantity, which is undesirable when dealing with defects such as porosity. The highlighted markers in the graph indicate the factor levels that have the most significant impact on increasing the response. This trend suggests the need to adjust process parameters toward lower values to achieve a reduction in porosity. In contrast, the main effects plot (Fig. 16) shows a decreasing trend, where changes in factor levels lead to a significant reduction in response values. This indicates that optimizing these factors accordingly can effectively minimize porosity and improve the overall process stability.

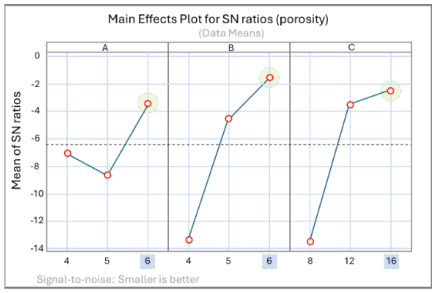

Fig. 15: Main effects plot for SN ratios of porosity.

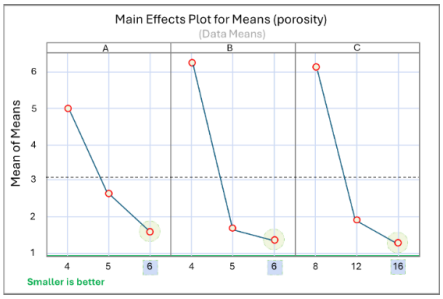

Fig. 16: Main effects plot for Means of porosity.

Versus Fits plot (Fig. 17) indicates that there is no correlation between the residuals and the sequence of data collection, confirming the absence of systematic errors. The approximate alignment (Histogram) with the expected distribution suggests that the residuals are normally distributed, supporting the validity of the model. The fluctuating pattern indicates that certain factor levels may still have some impact on variability, which should be

investigated further to refine the model, as reported in Versus Order plot (Fig. 17).

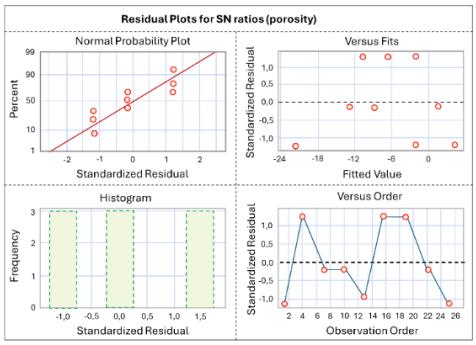

Fig. 17: Residual plots for SN ratios of porosity.

The costs associated with the gas flow rate were also analyzed as part of the individual optimization process. The objective, as determined by the signal-to-noise ratio criterion "Smaller is better," is to minimize these costs (Fig. 18). The most optimal parameter setting for cost reduction was identified as A3B2C1. Regarding factor B, the response values remained consistent across the evaluated levels.

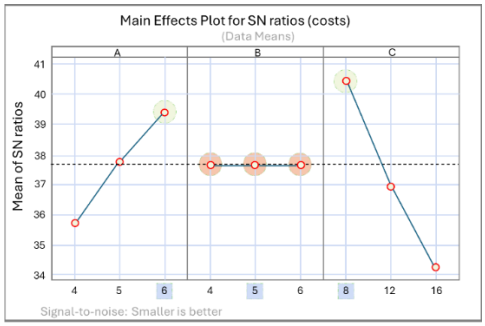

Fig. 18: Main effects plot for SN ratios of costs.

Based on the “Smaller is better” signal-to-noise ratio criterion, the optimal system configuration for minimizing cost was identified as A3B1C1. This selection was made by evaluating the influence of individual factors on the response variable, ensuring that the chosen parameter combination effectively reduces cost while maintaining stability (Fig. 19).

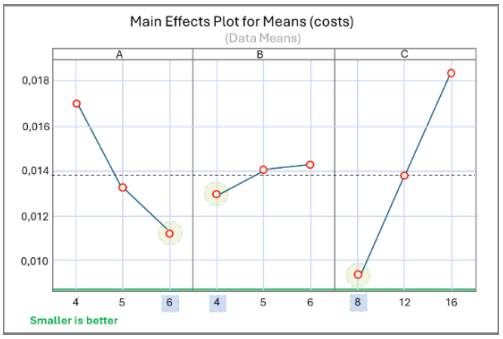

Fig. 19: Main effects plot for Means of costs.

3.2 Multi-objective optimization

To obtain comprehensive system-wide results, it was necessary to conduct a multi-objective factor analysis considering the evaluated responses. The grey relation grade (GRG) was calculated to establish the relative importance of each parameter and facilitate the selection of the optimal process conditions. The weightings of the responses were assigned based on their significance in the analysis, ensuring that their total sum equalled 1, thereby maintaining a balanced contribution to the final evaluation. Different weights were assigned to the parameters to reflect their impact on system optimization. Greater importance (0.3) was given to the parameters influencing width, height, and porosity, highlighting their critical role in achieving process efficiency (Tab. 11).

Tab. 11: Multi-objective factor analysis considering the evaluated responses.

	Grey relation coefficient				
	Norm width of bead	Norm heigh of bead	Norm penetration depth	Norm porosity	Norm costs
OWS/WFS/GFR	0.3	0.3	0.05	0.3	0.05
4/4/8	0.541578	0.609124	0.7465986	0.691416	0.666518
4/4/8	0.612123	0.663467	0.6393204	0.382029	0.666518
4/4/8	0.536678	0.333333	0.5453416	0.333333	0.666518
4/5/12	0.727813	0.850833	0.9216235	0.896665	0.444411
4/5/12	0.909897	0.637547	0.7470221	0.925351	0.444411
4/5/12	0.469403	0.817676	0.3988492	0.951171	0.444411
4/6/16	0.333333	0.627336	0.380856	0.957852	0.333333
4/6/16	0.364221	0.877521	0.3696323	0.93441	0.333333
4/6/16	0.764753	0.693215	0.618891	0.92	0.333333
5/4/12	0.418587	0.608493	0.5207592	0.658958	0.555721
5/4/12	0.483509	0.626667	0.54875	0.804467	0.555721
5/4/12	0.511656	0.908739	0.5657216	0.671002	0.555721
5/5/16	**0.839487**	**0.755627**	**0.8069853**	**0.792445**	**0.416364**
5/5/16	**0.779191**	**0.993238**	**0.8293451**	**0.915588**	**0.416364**
5/5/16	**0.755622**	**0.693215**	**0.6063536**	**1**	**0.416364**
5/6/8	0.672631	0.529518	1	0.726684	0.831567
5/6/8	0.910333	0.637547	0.7328881	0.924455	0.831567
5/6/8	1	0.657527	0.8139679	0.812686	0.831567
6/4/16	0.394575	0.975104	0.5003799	0.839859	0.499497
6/4/16	0.384117	0.833925	0.5358015	0.853375	0.499497
6/4/16	0.461305	0.628006	0.6971943	0.954023	0.499497
6/5/8	0.499934	0.691583	0.3611187	0.845064	1
6/5/8	0.554874	0.636856	0.3792111	0.756639	1
6/5/8	0.481547	1	0.3333333	0.775701	1
6/6/12	0.545781	0.742262	0.8139679	0.911217	0.666518
6/6/12	0.476113	0.659002	0.5758636	0.964629	0.666518
6/6/12	0.470917	0.609124	0.5618601	0.970513	0.666518

From the calculated GRG values (Tab. 12), the optimal parameter setting was identified, with the highest grey relational grade corresponding to the configuration 5/5/16 (OWS/WFS/GFR). This setting yielded the most favourable balance among the evaluated responses, demonstrating a grey relational grade best rank 0.777, 0.869 and 0.786. These results suggest that this specific parameter combination is the most suitable for optimizing welding performance while maintaining cost efficiency.

Tab. 12: The optimal grey relational grade results.

Grey relation grade OWS/WFS/GFR		Best rank
5/5/16	0.777435	7
5/5/16	0.86869	1
5/5/16	0.785787	6

The Grey Relational Grade (GRG) was utilized to analyze the main effects chart, identifying the optimal parameter settings as an overlay welding speed of 5 mm/s, a wire feed rate of 5 m/min, and a gas flow rate of 16 l/min. These findings validate the results obtained from the grey relational grade calculations, reinforcing the reliability of the optimization process (Fig. 20).

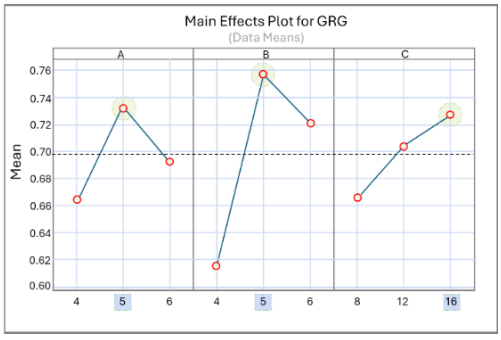

Fig. 20: Main effects plot for Grey Relation Grade.

4 CONCLUSION

Given these above parameters, OWS between 4 and 6 mm/s, WFS between 4 and 6 m/min and GFR between 8 and 16 l/min the results can be evaluated as follows. Based on the Taguchi method S/N ratios, it was found that the gas flow rate and overlay welding speed are significant factors for achieving the lowest costs. ANOVA for Means identified wire feed speed and gas flow rate as significant factors influencing the porosity of single-layer overlay welds. Conversely, ANOVA for Means for penetration depth classified overlay welding speed and wire feed speed as significant factors. For bead height, wire feed speed was identified as the only significant factor. Bead width was primarily influenced by welding speed and wire feed speed, while the shielding gas flow rate had an insignificant effect. Based on the grey relational grade in the multi-objective analysis, the most optimal parameters were identified as OWS = 5 mm/s, WFS = 5 m/min, and GFR = 16 l/min. The findings underscore the effectiveness of grey relation analysis as a decision-making tool for multi-objective optimization in overlay welding processes.

5 ACKNOWLEDGMENTS

This research was supported by the Slovak University of Technology (Program for support of young researchers No. 1345) and VEGA grant agency of the Ministry of Education, Research, Development, and Youth of the Slovak Republic under the project No. 1/0287/21.

6 REFERENCES

[Du 2023] Du, Z. and Li, L. Process Optimization, Microstructure and Mechanical Properties of Wire Arc Additive Manufacturing of Aluminum Alloy by Using DP-GMAW Based on Response Surface Method. Materials, 2023, 16(16), p. 5716. ISSN 1996-1944.

[He 2024] He, J., Liu, Y., and Zhang, X. Multi-Objective Optimization for Forming Quality of Laser and CMT-P Arc Hybrid Additive Manufacturing Aluminum Alloy Using Response Surface Methodology. Actuators, 2024, 13(1), p. 23. ISSN 2076-0760.

[Kazmi 2024] Kazmi, M. S., Ali, S., and Hussain, I. Wire Arc Additive Manufacturing of ER-4043 Aluminum Alloy: Effect of Tool Speed on Microstructure, Mechanical Properties, and Parameter Optimization. Journal of Materials Engineering and Performance, 2024, 33(10), pp. 5120–5133. ISSN 1059-9495.

[Kumar, P.B.K. 2021] Kumar, P.B.K., et al. Optimization of process parameters for turning machine using Taguchi super ranking method: A case study in valve industry. Materialstoday Proceedings, May 2021, Vol. 47, ISSN 2214-7853

[Lee 2020] Lee, H., Choi, S., and Park, J. Evaluation of Bead Geometry for Aluminum Parts Fabricated Using Additive Manufacturing-Based Wire-Arc Welding. Processes, 2020, 8(10), p. 1211. ISSN 2227-9717.

[Manikandan 2024] Manikandan, A., and Arumugam, M. Optimizing Cold Metal Transfer-Wire Arc Additive Manufacturing Parameters for Enhanced Mechanical Properties and Microstructure of ER5356 Aluminum Alloy Using Artificial Neural Network and Response Surface Methodology. Journal of Materials Engineering and Performance, 2024, pp. 1–20. ISSN 1059-9495.

[Mohd Mansor 2024] Mohd Mansor, M., Tan, C., and Idris, M. Integrated Approach to Wire Arc Additive Manufacturing (WAAM) Optimization: Harnessing the Synergy of Process Parameters and Deposition Strategies. Journal of Materials Research and Technology, 2024, 30, pp. 2478–2499. ISSN 2238-7854.

[Naveen Srinivas 2022] Naveen Srinivas, P., Kumar, R., and Reddy, R. Parametric Optimization and Multiple Regression Modelling for Fabrication of Aluminium Alloy Thin Plate Using Wire Arc Additive Manufacturing. International Journal on Interactive Design and Manufacturing, 2022, pp. 1–11. ISSN 2192-5769.

[Prasad 2024] Prasad, K., and Gupta, R. Experimental Investigation of Process Parameters of Cold Metal Transfer Welding-Based Wire Arc Additive Manufacturing of Aluminum 4047 Alloy Using Response Surface Methodology. Welding in the World, 2024, 68(11), pp. 2837–2852. ISSN 0043-2296.

[Pourkia, N. 2010] Pourkia, N., et al. The effect of Ti and Zr elements and cooling rate on the microstructure and tensile properties of a new developed super high-strength aluminum alloy. Materials Science and Engineering, July 2010, Vol. 527, ISSN 0921-5093

[Sarıkaya 2024] Sarıkaya, M., and Yılmaz, O. A Review on Aluminum Alloys Produced by Wire Arc Additive Manufacturing (WAAM): Applications, Benefits, Challenges, and Future Trends. Journal of Materials Research and Technology, 2024, 33, pp. 5643–5670. ISSN 2238-7854.

[Sesharao, Y. 2021] Sesharao, Y., et al. Optimization on Operation Parameters in Reinforced Metal Matrix of AA6066 Composite with HSS and Cu. Advances Materials Science and Engineering, July 2021, Vol. 2023, ISSN 1687-8442

[Shams 2024] Shams, A., and Saleh, M. Effect of Wire Arc Additive Manufacturing Process Parameters on Bead Geometry and Porosity Formation of 5356 Aluminum Alloy. International Journal of Materials Technology and Innovation, 2024, 4(2), pp. 39–45. ISSN 2215-1714.

[Singla 2024] Singla, S., and Verma, P. Microstructural and Mechanical Properties of Al-5356 Alloy Structures Fabricated Using Direct Energy Deposition (DED): In Pursuit of Optimizing Deposition Parameters. Materials Characterization, 2024, 216, p. 114321. ISSN 1044-5803.

[Wang, J. 2009] Wang, J., et al. Effects of trace Zr on the microstructure and properties of 2E12 alloy. Rare Metals, September 2009, Vol. 28, ISSN 1867-7185